Automated Pipeline for Multi-LiDAR Extrinsic Calibration: Experimental Evaluation and Performance Analysis

Surbhi Barnwal, Mansi Koshti, Salil Goel

Department of Civil Engineering, IIT Kanpur, Kanpur, India - surbhib20@iitk.ac.in, mansipk22@iitk.ac.in, sgoel@iitk.ac.in

Keywords: Calibration, LiDAR, Point Cloud, Registration, VLP16, ICP

Abstract

In recent years, 3D LiDAR (Light Detection and Ranging) has become a crucial sensor in various applications such as autonomous vehicles, robotics, object detection, precision forestry, and agriculture. However, specific LiDAR sensors, such as Velodyne VLP16, exhibit some drawbacks, such as a limited field of view and sparse data density, making them inadequate for certain specific applications. Hence, this research proposes a method for calibrating two VLP16 LiDAR sensors to improve coverage and reduce blind spots. The pipeline for performing the calibration begins with mounting LiDARs correctly in a rod at a specific orientation and distance, followed by the selection of multiple sites for data collection, then performing a registration algorithm for estimating calibration parameters, and then an accuracy assessment of the calibrated point clouds. The registration algorithm used here is a modified version of ICP (Iterative Closest Point), which overcomes the need for initialization and eliminates manual intervention in installing targets or retro-reflectors. Finally, we evaluated the accuracy of the fused point cloud collected in an open environment using two calibrated Velodyne VLP16 sensors. For accuracy assessment, we used the PCA eigenvalue and RMSE value to observe how tightly point clouds are fused. As a calibration result, we got the orientation and translation parameters, which are used to achieve the common coordinate system, and accomplished calibration accuracy up to single-digit precision from all the experimental sites. Now the system of two calibrated VLP16 sensors will provide higher coverage and increased data density and might be useful for forest applications.

1. Introduction

Over the last few decades, LiDAR has become an emerging sensor for a wide range of applications, including autonomous vehicles, robotics, object identification, mapping, precision agriculture, and forest biomass estimation for accurate horizontal and vertical distance measurement (Jiao et al., 2019). Nevertheless, a single low-cost LiDAR is insufficient for these applications due to its limited vertical field of view and sparse data density. As a result, it becomes important to calibrate multiple sensors to obtain optimum coverage of the surroundings. There are two types of calibration performed in LiDAR: extrinsic and intrinsic calibration. Intrinsic calibration mainly focuses on the internal characteristics of the LiDAR sensors, which ensure that each horizontal beam of the LiDAR, vertical angle, and range offset are properly calibrated. Here, we assumed that intrinsic calibration is performed during the manufacturing process (Lee and Chung, 2022). Extrinsic calibration is the method of determining the relative position and rotation between the sensors. To fuse the sensor information into a single coordinate system, all sensors have to be calibrated relative to the chosen common frame. Through the calibration of two sensors' measurements, we align each sensor's coordinate system with a common reference frame and fuse the point cloud of both sensors (Heide et al., 2018).

Numerous studies explored LiDAR-camera calibration and camera-camera extrinsic calibration, reflecting a significant amount of research in these areas. However, there is increased demand for research addressing extrinsic multi-LiDAR calibration for various applications. Extrinsic calibration is categorized into two categories, i.e., offline and online. Offline calibration is considered a registration problem where a cost function is minimized (Heide et al., 2018; Maye et al., 2016). It involves estimating the extrinsic parameters of multiple LiDARs, either through manual interventions or automated processes. Calibration methods using artificial calibration objects require manual processes for making the objects and for placing them in the scenes(Gao and Spletzer, 2010; Pusztai et al., 2018; Underwood et al., 2007). Additionally, we must create a calibration room each time calibration work is conducted. Consequently, automatic registration is employed to estimate the calibration parameter, which involves the registration of point clouds based on surrounding features as well as removing the need to find an initial set of parameters. Researchers leverage linear or planar features, and any objects lie in the surrounding environment where sensors are kept. A number of registration algorithms have already been developed in the market, such as Normal Distributions Transform (NDT), Iterative Closest Point (ICP), and its different versions, which can be implemented for extrinsic calibration. In contrast to offline calibration, where calibration is performed separately and applied later (Besl and McKay, 1992; Gao and Spletzer, 2010).

Initially, the calibration of LiDAR sensors was performed using retro-reflectors and manual targets within scenes, referred to as the manual registration approach(Jiao et al., 2019; Zhou et al., 2018). Gao and Spletzer, (2010) proposed an algorithm to calibrate multiple LiDARs using point constraints provided by retro-reflective tapes. For LiDAR-camera calibration, (Zhou et al., 2018)demonstrated a technique to establish line and plane constraints between the two sensors using a chessboard, while Liao et al., (2018) introduced a toolkit using an arbitrary polygon, offering greater versatility. However, some studies have opted to use surrounding features instead of manual targets or retroreflectors to solve the multi-LiDAR calibration problem. For example, Xie et al., (2018) presented a general solution to jointly calibrate multiple cameras and LiDARs in environments with pre-built features, such as Apriltags. Choi et al., (2016) determined the spatial offset of dual 2D LiDARs by leveraging the appearance of two orthogonal planes. Lee and Chung., (2022) employed orthogonal planes for registration and automated the registration method to address multi-LiDAR calibration challenges.

This contribution has been peer-reviewed. The double-blind peer-review was conducted on the basis of the full paper.
https://doi.org/10.5194/isprs-annals-X-4-2024-37-2024 | © Author(s) 2024. CC BY 4.0 License.

The current state of research in the field indicates a significant gap regarding LiDAR-LiDAR automated calibration, with just a few works addressing this topic. Furthermore, comprehensive accuracy assessments have been largely overlooked, leaving uncertainties regarding the reliability of fused data obtained through multi-LiDAR systems. The first objective of the study is to perform an offline automatic calibration of two low-cost VLP 16 LiDAR to achieve enhanced coverage of the surroundings. The calibration output will be the calibration parameter and the fused point cloud from both sensors. The outcome of the calibration task will be referred to as either a calibrated point cloud or a fused point cloud derived from two synchronized and calibrated sensors. The second objective of the paper is to evaluate the accuracy of the estimated calibration parameters through the accuracy evaluation of the fused point cloud. The following section explains the experimental setup and methodology adopted. This is followed by results and an accurate evaluation of the estimated parameters. Finally, the conclusions of the paper are presented in section 4.

2. Datasets and Methodology

2.1 Hardware setup

We mounted two low-resolution Velodyne VLP16 for this study on a rod (Figure 1). This was done to improve the effective coverage of the two sensors combined. This is only one of the specific configurations, and any other configuration could also be used here, depending on the intended application. The two sensors are connected to a common Computer, and a software-based time synchronization is performed. We propose an automatic calibration process that relies on the presence of external features for successful calibration. The type and distribution of these features affect the calibration performance. To analyze the calibration performance in different conditions, we select five different environments, of which four are indoors, which is used for estimation of calibration parameters, and one is an outdoor environment, which is used for validation. The following section provides the details of the experimental sites.

Figure 1. Experimental Setup for two VLP16 sensor.

2.2 Data collection

As explained earlier, five experimental sites were chosen. It is to be noted that no artificial targets are installed by the authors at any of these sites, and data is collected in their natural conditions. These sites are enclosed rooms containing engineering features such as chairs, tables, almirahs, and walls, representing planar, linear, or edge structures. Further, to implement calibration parameters and fuse the measurements, we again collected datasets in an open environment where we witnessed cars, trees, walls, and poles. Four indoor environment sites were used to find the best calibration parameter, and an open environment site was used to implement the calibration parameter. Measurements are taken from two low-cost Velodyne VLP16 synchronized sensors by keeping the sensors at the center of the enclosed space. Data collection was done using the Robot Operating System (ROS) platform. Following data collection, it was processed and converted into standard point cloud format using MATLAB and Cloud Compare. The specification of Velodyne LiDAR Puck™, is described in the datasheet (Velodyne LiDAR, 2019). The sensors' specifications and their setup are mentioned below in Table 1.

Specification	Velodyne VLP16
Channels	16
Range	100 m
Vertical FOV	-15^0 to $+15^0$ (30^0)
Horizontal FOV	360^0
Vertical angular resolution	2.0^0
Horizontal angular resolution	$0.1^0 – 0.4^0$
Range accuracy	±0.03 m
Point per second	396, 000

Table 1 Specification of Velodyne VLP 16 sensor.

2.3 Pre-processing of the point cloud

Datasets obtained from two synchronized VLP16 are represented as the source and target point clouds. The sensor kept at the top of the rod is called the target sensor, while another sensor kept at inclination is considered as the source sensor (Figure 1). In this study, we solved the calibration problem using an automatic registration problem where we did not use any retroreflector or physical targets. After data collection, we removed the noise and outliers in the point cloud due to dust, smoke, or other environmental conditions. For pre-processing, we used statistical and radius noise removal filters as well as voxel grid down-sampling. We followed the tutorial on point cloud outlier removal provided by Open3D documentation. Voxel grid sampling down sampled the point cloud to reduce the number of points. It is implemented in the raw point cloud obtained from synchronized LiDAR sensors, which contain a large number of data points, all of which may not be useful for registration. We created a voxel of the point cloud of size 5 cm for light sampling. Further, having a large number of data points in the point cloud may significantly increase the computation time. Further, a statistical outlier removal (SOR) filter was implemented to the downsampled point cloud to remove the outlier. The SOR filter, as described in the Point Cloud Library documentation, is used to remove outliers from point cloud data. It removes points that are further away from their neighbors compared to the average for the point cloud. It takes two input parameters: nearest neighbor and standard ratio. The number of neighbors is taken as 10, and the standard ratio is selected as 2.0. As number of neigbour increase in statistical outlier, no. of outlier decreases. Nearest neighbor allows to specify how many neighbors are taken into account to calculate the average distance for a given point, and standard ratio allows setting the threshold level based on the standard

deviation of the average distances across the point cloud. The lower this number is, the more aggressive the filter will be. Additionally, a radius outlier is performed to remove the points with few neighbors in a given sphere (Uddin et al., 2022).

Furthermore, the K-dimensional (K-D) Tree is also applied to the denoised point cloud to find the correspondence pair of the point cloud. KDTree queries involve searching for the nearest neighbors of a specified point within a K-D Tree data structure. It is a binary tree data structure commonly used in Computer science to search k-dimensional points efficiently. The K-D Tree is constructed by recursively splitting the space into two regions based on the median of the points in that region along a certain dimension. It is used to perform a nearest-neighbor search, which helps us find the correspondence between two point clouds. Correspondences refer to the set of similar point pairs in the two point clouds. Once the correspondence is identified, an iterative process reduces the distance between these points. Accurately identifying and matching these unique correspondences is important for precise registration.

2.4 L-M optimization

After correspondence is identified and matched, the result of registration is optimized using Levenberg-Marquardt (L-M) optimization. The L-M algorithm is utilized in point cloud registration to solve the challenges of accurately aligning two-point clouds, which have limitations such as low overlap, noise and outliers, and complex surroundings. The L-M algorithm also overcomes the problem of local minima created during ICP registration by obtaining global minima. The algorithm enhances the results of point cloud registration by providing a robust and efficient approach to solving non-linear least squares problems, which are common in aligning point clouds (Fitzgibbon, 2003).

The update formula for the parameters p in the LM algorithm is:

$$p_{k+1} = p_{k-} \ (J^t J + \lambda I)^{-1} J^T r \qquad (1)$$

Where:

p_{k+1} = Updated parameter vector at iteration k+1
p_{k+1} = Parameter vector at iteration k
I = Identity matrix
J = Jacobian matrix of derivatives of the residuals with respect to the parameters
r = Residual vector
λ = Damping parameter

2.5 Accuracy assessment for the registration result

After solving the calibration problem using the registration method, we obtained a transformation matrix, a registered/fused point cloud from the calibrated sensor, and a Root Mean Square Error (RMSE) value from each experimental site (enclosed indoor environment). As we are solving the calibration problem using the registration method, the transformation matrix will also be referred to as the calibration parameter. Since the calibration parameters are computed from four indoor sites, it is possible to estimate the variation in these parameters. Note that the calibration parameters should ideally be constant, irrespective of where the data is collected, as long as the hardware configuration remains the same. However, we may get slightly different calibration parameter values due to the range error, perturbation of the sensor, non-ideal environmental conditions, and calibration algorithm. Additionally, to assess the calibration parameter variability across different experimental sites, the standard deviation, along with the mean, is computed.

RMSE

RMSE is a metric used to quantify the accuracy of the registration process by measuring the differences between corresponding points in two point clouds (source and target point cloud).
RMSE can be calculated as,

$$\text{RMSE} = \sqrt{\frac{1}{n}\sum_{i=1}^{n}\left(s_i - t_j\right)^2} < \sigma, \ (1 \leq j \leq m) \qquad (2)$$

where s_i is the nearest point in the target dataset of t_j in the source dataset,

m and n are the numbers of points of Source and Target point cloud, respectively, and

σ is the threshold for the minimum distance between the two datasets.

2.6 Assessment of fused Point Cloud Accuracy in Open Outdoor Environments

We used Principal Component Analysis (PCA) eigenvalues and RMSE to evaluate the fused point cloud of an open outdoor environment using four sets of calibration parameters achieved from four enclosed indoor sites. For this, individual features such as poles, tree trunks, and walls have been segmented. A line and a plane have been fitted for the linear and planar features. A line has been fitted to the pole (as the pole is the linear feature), and a direction vector has been calculated along the fitted line to know the maximum variance along the fitted line. For the wall, a plane fitted to the segmented wall point cloud to know how well points are spread in x, y, and z directions. For this, eigenvalues as λ1, λ2, and λ3 are calculated for pole and wall. We could not fit a cylinder or other shape to the tree trunk due to the partial scanning by both sensors. Apart from the eigenvalues, we also calculated the direction vector for each point cloud collected from each sensor after applying the calibration parameter. The direction vector determines how well sensors are calibrated in the angular direction. Furthermore, we calculated RMSE for the segmented features using the K-D Tree as well.

PCA eigenvalue and eigen vector computation

The PCA eigen values derived from the data's covariance matrix, obtained through eigen decomposition or singular value decomposition, capture the optimal fitting directions (principal components) that are orthogonal to each other. In this study, PCA eigenvalues were employed to evaluate the rotational alignment of point clouds collected from individual sensors after calibration, while RMSE determined the effectiveness of fusion/calibration in terms of translational shift.

The eigenvalues and eigenvectors of a matrix A can be calculated using the characteristic equation:

$$\det(A - \lambda I) = 0 \qquad (3)$$

where λ is the eigenvalue, I is the identity matrix, and det denotes the determinant of the matrix.

Once the eigenvalues are obtained, the corresponding eigenvectors can be found by solving the equation:

$$(A - \lambda I)v = 0 \qquad (4)$$

Where v is the eigen vector corresponding to the eigenvalue λ.

The overall methodology is presented using a flowchart, showing the different steps for finding the best calibration parameter (Figure 2).

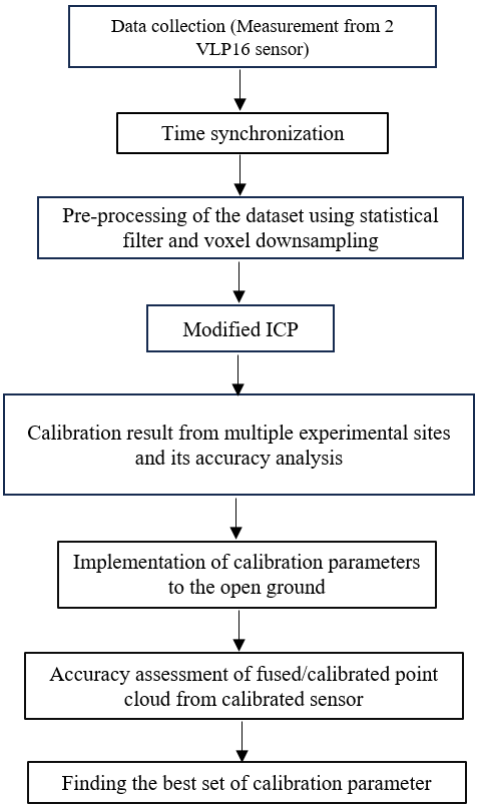

Figure 2. Flowchart showing the overall method for finding the best calibration parameter.

3. Result and discussions

3.1 Pre-processing result

The synchronized point cloud data from two LiDAR sensors were collected across four different experimental sites, all of which were enclosed indoor environments. These sites included a Lab, a Computer room, an Instrument room, and an Office room. The raw data from these sensors consisted of a dense collection of 3D points, representing the surfaces within these environments.

Once the data was collected, it underwent pre-processing to eliminate the noise and outliers. Figure 3 illustrates the significant reduction of unwanted noisy points following the preprocessing steps across all four site measurements. The bar graph depicts the reduction of point cloud data for two sensors in four different rooms after pre-processing, which removes noise, outliers, and unwanted points, which is not useful for the registration. The Lab and Computer rooms show higher data density both before and after pre-processing than the Instrument and Office room due to the larger room size.

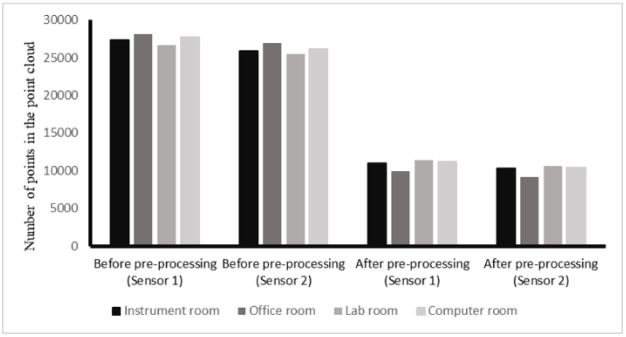

Figure 3. Comparison of point cloud density before and after pre-processing from two LiDAR sensors.

3.2 Calibration result

The automatic registration algorithm was implemented in the denoised point cloud, which yielded four sets of transformation matrices, also called calibration parameters. Moreover, the registered point cloud and its corresponding RMSE were determined, with the RMSE providing a measure of the registration or calibration accuracy with which the point clouds from the synchronized sensors were registered.

Table 2 shows that the RMSE value was lower for the Instrument room and Office room at 0.068 m and 0.062 m, respectively; this suggests a more accurate registration of the point cloud data and better calibration of the sensors. This could be attributed to specific characteristics of the rooms, which may have facilitated a more precise calibration parameter because these rooms are of small size, and features and objects of the room can be identified easily by the sensor.

Conversely, the Computer and Lab rooms recorded slightly higher RMSE values of 0.072 m and 0.078 m, indicating a lesser degree of registration accuracy. These differences may come from the different features that were scanned through the sensor and the larger size of the room, due to which few features couldn’t be identified due to the limited range of the sensor. Understanding these variances is crucial for improving point cloud registration techniques and adapting them to the unique conditions presented by each experimental site.

In an ideal condition, the optimal site of the best calibration result comprises an enclosed space with distinguished features and objects that can be completely scanned by the sensors.

Experimental site	**Instrument room**	**Office room**	**Lab room**	**Computer room**
RMSE (in meters)	0.069	0.062	0.078	0.072

Table 2. RMSE value (in meters) computed during registration for each indoor experimental site.

In Figure 4, the RMSE value is plotted with respect to the number of iterations for four sets of experimental sites. The plot indicates that the RMSE values varied from 0.13 to 0.06 m throughout the iterations. Furthermore, it was noted that all experimental locations had many local minima and fluctuations up to the 17h or 18th iteration, but after that, the RMSE values get saturated. This pattern indicates that using a registration procedure and LM optimization helps achieve the global minimum. Throughout the process, the Instrument and Office rooms consistently demonstrate lower RMSE values, indicating a more accurate registration compared to the Lab and Computer rooms results.

This contribution has been peer-reviewed. The double-blind peer-review was conducted on the basis of the full paper.
https://doi.org/10.5194/isprs-annals-X-4-2024-37-2024 | © Author(s) 2024. CC BY 4.0 License.

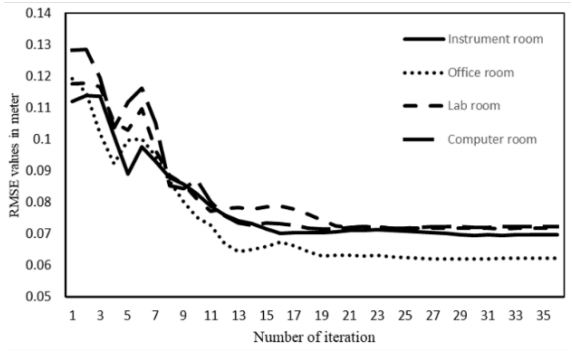

Figure 4. RMSE variation with respect to the number of iterations across four sites.

3.2 Analysis of the variation in translation and rotation parameter

We computed the variation in translation and rotation derived from the transformation matrix result of four experimental sites. In Table 3, we depicted the mean and Standard deviation (SD) of translation along the x, y, and z axes, as well as the roll, pitch, and yaw values.

The statistical analysis indicates minimal dispersion in translation across the x, y, and z axes, suggesting precise consistency in these measurements as observed by SD. However, there is a minor variation in the rotational values (roll, pitch, and yaw), which could potentially be attributed to constraints in the quality of the point cloud from the VLP 16 sensor or calibration algorithm.

	t_x	t_y	t_z	Roll	Pitch	Yaw
	In meters			In degrees		
Mean	0.054	0.200	0.349	9.704	0.434	2.583
S.D.	0.001	0.005	0.014	1.185	0.480	0.877

Table 3. Mean and SD for the translation and rotation values.

Figure 5.a and b display the values of tx, ty, tz, and roll, pitch, and yaw in meter and degree, respectively, in the form of a bar graph so that we can visualize the similarity of the translation and rotation values computed for four experimental sites. Here, t_x, t_y, and tz are translations along the x, y, and z-axis, and roll, pitch, and yaw are the rotations along the x, y, and z directions, respectively. In Figures 5a and b, the x-axis depicts the translation values in meters and rotation values in degrees, respectively.

From Figure 5a, we can observe that translation along the x, y, and z axes is consistent for all the experimental sites; however, for the rotation parameter, the computer room depicts a slight variation in roll value, while the computer room and Lab room represent slight variation in yaw value (Figure 5b).

Ideally, consistent translational and rotational values are expected across all experimental sites. However, we observed some noticeable discrepancies in rotational values computed for the Laboratory and Computer rooms. This discrepancy may be contributed from the critical selection of correspondences necessary during registration, which is influenced by the available features and the size of the rooms as well as the extrinsic perturbation. The computer room and Lab room were larger in size compared to the Instrument room and Office room, due to which a few features, which were present at a farther distance from the sensor, could not be captured well, which affected the registration and consequently led to the observed rotational variations.

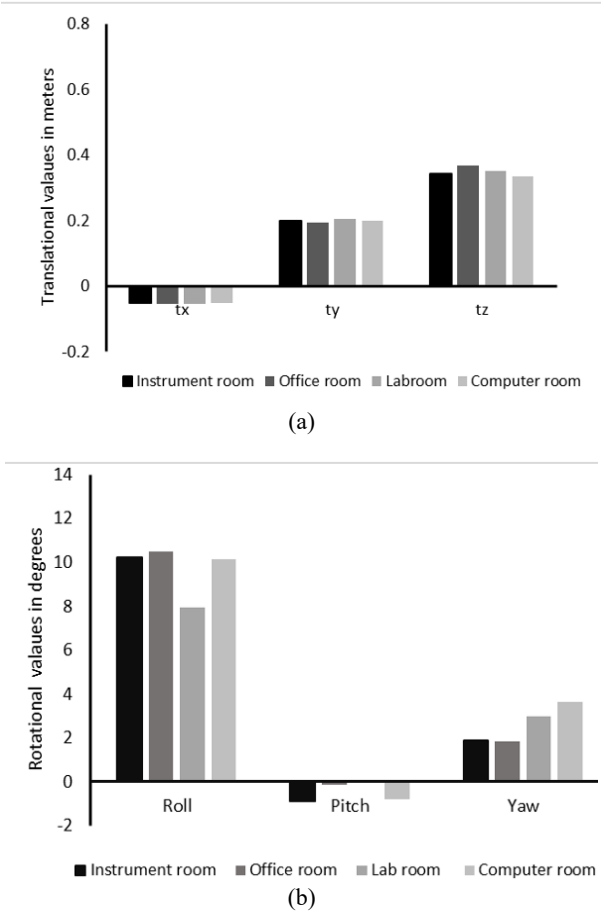

Figure 5. Translation (a) and rotation values (b) variation across four experimental sites.

3.3 Analysis of the fused point cloud for the open environment from calibrated sensors

Finally, after getting transformation matrices from four experimental sites, we implemented these calibration parameters to the point cloud of the open environment collected from the setup of two synchronized Velodyne VLP16 sensors. Here, to avoid confusion, we will refer to the transformation matrix as the calibration matrix as we are performing the calibration problem by means of the registration method. In this study, a calibrated point cloud using one of the experimental site’s calibration parameters is presented only to visualize the differences in data appearance in a single sensor and a calibrated sensor. Additionally, the shift in the point clouds resulted from two individual sensors before and after calibrations are also presented.

3.3.1 Comparison of single sensor and dual sensors measurement

Analysis of the single sensor point clouds (figure 6a) reveals a notably low data density, which significantly improves after calibration (figure 6b). Consequently, adopting a multi-sensor

approach facilitates enhanced data collection, offering improved detail and mitigating issues associated with occlusion.

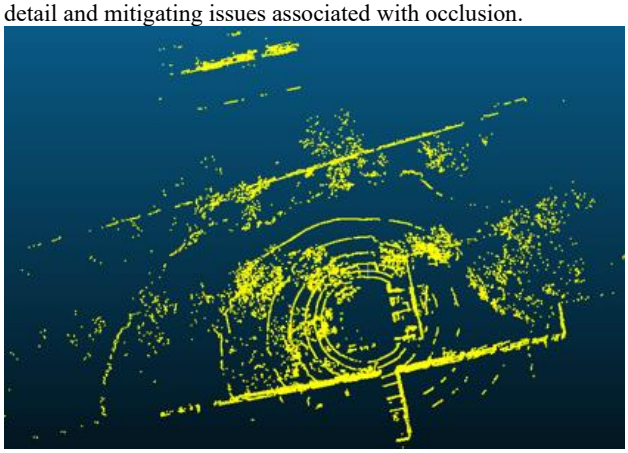

(a)

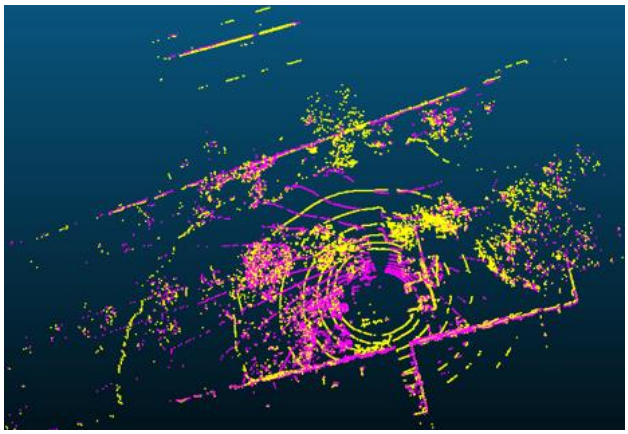

(b)

Figure 6. Point cloud from the one sensor (a) and dual calibrated sensor (b).

3.3.2 Detailed analysis of the fused point cloud from the calibrated sensor

To show the shift between the sensor's data before and after calibration, in Figure 7, a few features from the fused point cloud of the open environment were highlighted. The pre- and post-calibration shifts are most effectively depicted in a 3D visualizer. However, due to the constraints of this paper, we are limited to exhibit them solely through 2D photographs. Figure 7a presents a segmented wall pre- and post-calibration side by side for direct comparison, while Figure 7b shows a top view of three segmented cars (before and after calibration), demonstrating the improved alignment of the point cloud after calibration. Further, Figure 7c compares the tree trunk before and after calibration to showcase that, there is no shift in the fused point cloud after registration. Figure 7d also illustrates the same pattern for linear feature as pole as found in walls, cars, and trees. For the calibration of the sensors, the Instrument room calibration parameter.

The visual comparison in Figure 7 confirms the effectiveness of sensor calibration, showing minimal or no shifts in segmented features after calibration, indicating successful alignment and effective calibration of the setup of two synchronized sensors which increases the coverage and data density.

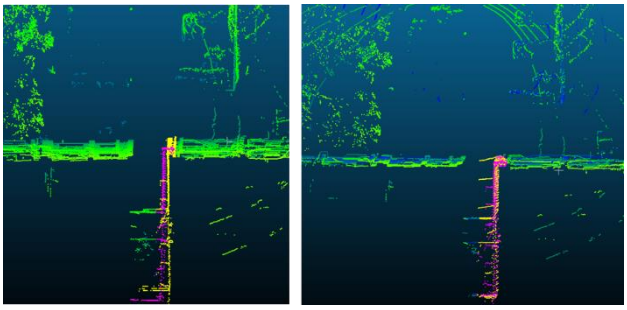

(a)

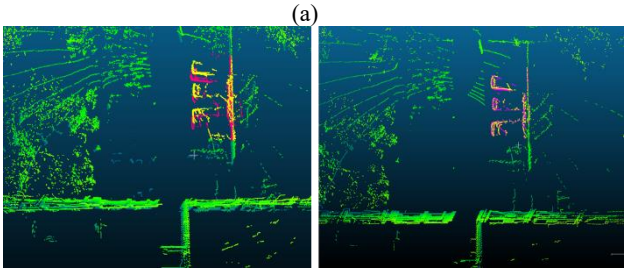

(b)

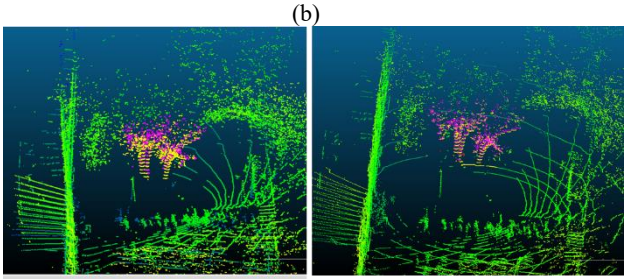

(c)

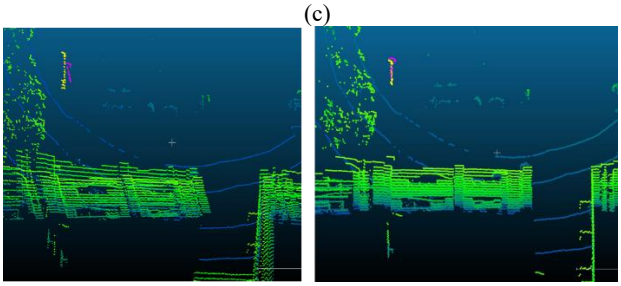

(d)

Figure 7. Segmented features such as Wall (a), Cars (b), part of the tree trunk (c), and Pole (d) before (left) and after (right) calibration.

3.4 Accuracy assessment for the calibrated point cloud

We evaluated the calibrated point cloud quality through two methods: RMSE, for segmented point clouds of features present in the surroundings of an open environment, indicates alignment precision in translation, while PCA eigenvalues and eigenvectors assess angular discrepancies between the two point clouds.

3.4.1 RMSE Analysis

RMSE values for the segmented Wall, Pole, and Tree are shown in the form of a bar graph (Figure 8). and the direction vector between the source and target segmented point clouds (Pole and Wall) obtained from the source sensor (kept at an incline) and the target sensor (positioned at the top) after the calibration process, as shown in Table 4.

In Figure 8, RMSE value is shown for various features as Pole, Wall, and Tree trunk, segmented from calibrated sensors. Fusion of the point clouds for two sensors was performed using the calibration result of four experimental sites, which shows the

lowest RMSE value for the Instrument room and Office room and a higher value for the Lab room and Computer room for all the segmented features.

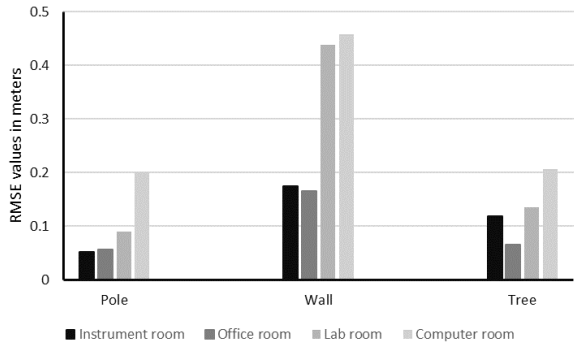

Figure 8. RMSE values for segmented features (Pole, Wall, and Tree) across four different environments (Instrument room, Office room, Lab room, and Computer room).

3.4.2 Eigenvalue eigenvector analysis

In Table 4, the value computed from PCA and the angle between the direction vector are shown for a linear feature as a pole and a planar feature as a wall. Eigenvalues are unitless, while the angle is shown in degrees. λ1, λ2, and λ3 are variance of points in x, y, and z direction, respectively. Segmented Pole point clouds exhibit the maximum variation in the x direction as it is a one-dimension feature for the Instrument and Office room. However, for the Lab room and Computer room, we observed a nonzero value in λ2, which means that the fused point cloud exhibits a slight deviation in the y direction. Additionally, the angle between the direction vector is the least for the Instrument room and Office room, while for the Lab room and Office room, a higher value is witnessed. Ideally, the angle between the direction vector of the target and the transformed source point cloud is zero, but since there is a small shift in the orientation, it is computed as a small non-zero value. Further, the segmented wall is a planar feature, it should show a non-zero value in the x and y directions and 0 in the z direction if it is a perfect plane. However, we observed a significant non-zero value in the z-direction for the Lab room and Computer room, indicating that points of the segmented wall are not fused properly (Table 4).

		Instrument room	**Office room**	**Lab room**	**Computer room**
Pole	λ1	0.543	0.54	0.537	0.541
	λ2	0	0	0.02	0.004
	λ3	0	0	0	0
	angle between direction vector	0.725	0.647	1.412	0.856
Wall	λ1	4.256	4.374	4.481	4.462
	λ2	2.007	2.198	2.128	2.007
	λ3	0.001	0.002	0.021	0.047
	angle between direction vector	0.434	0.606	1.696	1.596

Table 4. Illustrates the eigenvalues and angle between the direction vector (in degrees) for line feature (Pole) and plane feature (Wall).

3.4.3 Comparative analysis of the calibration parameter for four sites

We performed the comparative analysis of the result of four experimental sites and for this, three distinct features: a pole, a vertical wall, and a section of a tree trunk segmented and from the measurements of the calibrated sensors and visualized (Figure 9). All the segmented features reveal that, based on Instrument room and Office room calibration parameters, these segmented features are well aligned compared to the calibration result of the Computer room and Lab room, indicating that sensors are effectively calibrated using Instrument and Lab room calibration parameters.

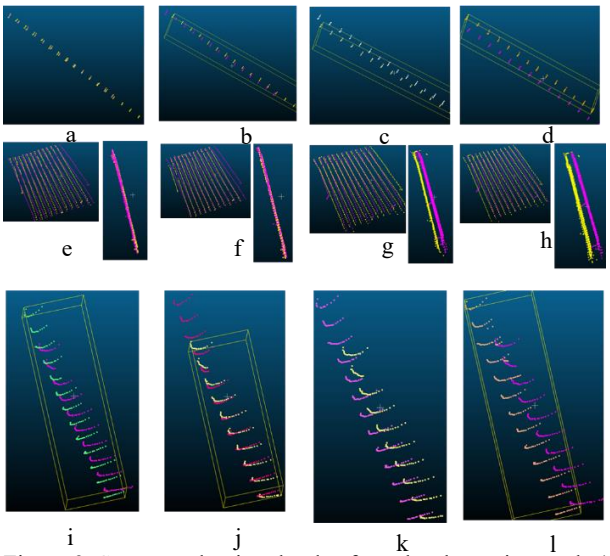

Figure 9. Segmented point clouds of a pole, shown in panels (a-d). Panels (e-h) illustrate a wall's point cloud, presented horizontally and vertically, and Panels (i-l) feature a section of a tree trunk, fused with calibration parameters from Instrument room, Office room, Lab room, Computer room (left to right)

In summary, the calibration parameters for the Instrument room and Office room prove to be effective, exhibiting minimal registration errors (see Table 2), the least spread of the point cloud in an incorrect direction, and small non-zero angles between vectors for all segmented features, compared to the Lab room and Computer room (refer to Table 4). Additionally, a similarity is observed between the translational and rotational parameters of the Instrument room and Office room, contrasting with those of the Lab room and Computer room (see Figure 5). Visualization of the segmented feature, as shown in Figure 9, also indicates the best result from the calibration parameter of the Instrument room and Office room. Consequently, either the Instrument room or Office room-based calibration parameters can be utilized to merge the point cloud collected from two synchronized sensors for further processing.

4. Conclusion and future works

The paper presents a comprehensive study on the multi-LiDAR extrinsic calibration for improving coverage and data density in capturing the surrounding environment using two Velodyne VLP16 LiDAR sensors mounted in a rod. This study employed a modified version of ICP that significantly eliminates the need for manual intervention by employing an automated registration algorithm along with the LM optimization technique, which optimizes the result. Data collection was performed across four enclosed indoor environments just to ensure that we were getting

a significantly similar value from each experiment site. Further, to assess the calibration's effectiveness in diverse conditions, we collected the dataset in an open environment. The results demonstrated a notable improvement in data density and coverage, particularly advantageous for forestry applications and other outdoor environments.

Finally, to analyze the result from the calibration parameter, we did a thorough accuracy assessment using various statistical methods, including PCA eigenvalues and RMSE, which revealed minimal dispersion in translation and slight variations in rotation attributed to the quality of the point cloud data. These metrics confirmed the high accuracy of the calibration process, with particular success in the Instrument and Office rooms, suggesting that the calibration parameters are significantly reliable. The paper also discusses the challenges of capturing features at a distance in larger rooms, which can negatively impact registration and lead to errors in calibration parameters.

In conclusion, this study advances the field of LiDAR sensor calibration by offering a robust and automated solution that enhances environmental coverage and point cloud density. This development holds great potential for improving the performance of multi-LiDAR systems in a wide range of applications. Future work may include the third sensor to get a complete view of the environment so that the final data comprised of the three sensors can be used for data collection in a forest environment.

5. References

Besl, P.J., McKay, N.D., 1992. A Method for Registration of 3-D Shapes. *IEEE Trans Pattern Anal Mach Intell* 14. https://doi.org/10.1109/34.121791.

Choi, D.G., Bok, Y., Kim, J.S., Kweon, I.S., 2016. Extrinsic Calibration of 2-D Lidars Using Two Orthogonal Planes. *IEEE Transactions on Robotics* 32. https://doi.org/10.1109/TRO.2015.2502860.

Heide, N., Emter, T., Petereit, J., 2018. Calibration of multiple 3D LiDAR sensors to a common vehicle frame, *in: 50th International Symposium on Robotics, ISR* 2018.

Fitzgibbon, A.W., 2003. Robust registration of 2D and 3D point sets, in: Image and Vision Computing. https://doi.org/10.1016/j.imavis.2003.09.004.

Gao, C., Spletzer, J.R., 2010. On-line calibration of multiple LIDARs on a mobile vehicle platform, in: *Proceedings - IEEE International Conference on Robotics and Automation*. https://doi.org/10.1109/ROBOT.2010.5509880.

Jiao, J., Liao, Q., Zhu, Y., Liu, T., Yu, Y., Fan, R., Wang, L., Liu, M., 2019. A novel dual-lidar calibration algorithm using planar surfaces*, in: IEEE Intelligent Vehicles Symposium, Proceedings*. https://doi.org/10.1109/IVS.2019.8814136.

Lee, H., Chung, W., 2022. Extrinsic Calibration of Multiple 3DLiDAR Sensors by the Use of Planar Objects. *Sensors* 22. https://doi.org/10.3390/s22197234.

Liao, Q., Chen, Z., Liu, Y., Wang, Z., Liu, M., 2018. Extrinsic Calibration of Lidar and Camera with Polygon, in: 2018 *IEEE International Conference on Robotics and Biomimetics, ROBIO* 2018. https://doi.org/10.1109/ROBIO.2018.8665256.

Maye, J., Sommer, H., Agamennoni, G., Siegwart, R., Furgale, P., 2016. Online self-calibration for robotic systems. *International Journal of Robotics Research* 35. https://doi.org/10.1177/0278364915596232.

Point Cloud Library. Removing outliers using a StatisticalOutlierRemoval filter. Retrieved from https://pointclouds.org/documentation/tutorials/statistical_outlier.html (28 March 2024).

Point cloud outlier removal - Open3D 0.18.0 documentation. http://www.open3d.org/docs/release/tutorial/geometry/pointcloud_outlier_removal.html (20 March 2024).

Pusztai, Z., Eichhardt, I., Hajder, L., 2018. Accurate calibration of multi-lidar-multi-camera systems. *Sensors (Switzerland)* 18. https://doi.org/10.3390/s18072139.

Uddin, S., Haque, I., Lu, H., Moni, M.A., Gide, E., 2022. Comparative performance analysis of K-nearest neighbour (KNN) algorithm and its different variants for disease prediction. *Sci Rep* 12. https://doi.org/10.1038/s41598-022-10358-x.

Underwood, J., Hill, A., Scheding, S., 2007. Calibration of range sensor pose on mobile platforms, *in: IEEE International Conference on Intelligent Robots and Systems*. https://doi.org/10.1109/IROS.2007.4398971.

Velodyne LiDAR., 2019. Puck™ Datasheet. https://velodyneLiDAR.com/wp-content/uploads/2019/12/63-9229_Rev-K_Puck-_Datasheet_Web.pdf (20 March 2024).

Wolfram MathWorld. Levenberg-Marquardt Method. https://mathworld.wolfram.com/Levenberg-MarquardtMethod.html (28 March 2024).

Xie, Y., Shao, R., Guli, P., Li, B., Wang, L., 2018. Infrastructure Based Calibration of a Multi-Camera and Multi-LiDAR System Using Apriltags, *in: IEEE Intelligent Vehicles Symposium, Proceedings*. https://doi.org/10.1109/IVS.2018.8500646.

Zhou, L., Li, Z., Kaess, M., 2018. Automatic Extrinsic Calibration of a Camera and a 3D LiDAR Using Line and Plane Correspondences, *in: IEEE International Conference on Intelligent Robots and Systems.* https://doi.org/10.1109/IROS.2018.8593660.